which is the viscosity obtained by a disk stability estimate[11]. The disk mass is decreased as material spreads onto the Earth or past a_{Roche}.

Figure 1 shows the evolution of I, a and σ as the Moon recoils from a disk of mass $M_{disk} = 0.75\ M_{Moon}$, assuming that $a_o = 3.5R_|$ and $a_1 = 4.1R_|$. The resulting maximum inclinations are 12.3° and 14.5° for $t_{spread} = 37$ and 50 years, respectively. The timescale, t_{IVR}, for growth in a due to the IVR is regulated by the location of the disk edge to be comparable to t_{spread}. As the IVR nears the edge of the disk, the back torque from the Moon retards the disk's tendency to spread, and the IVR begins to migrate out of the disk. But as this occurs, the back torque on the disk is decreased, allowing increased spreading of disk material outward, until once again the IVR is in the disk. In this manner, the location of $r_{disk}(t)$ and the location of the IVR move in lock step. Once $r_{disk} = a_{Roche}$, the edge of the continuous disk does not advance because material spreading beyond a_{Roche} can accrete into discrete objects which are not effective at sustaining wave action. The continued outward migration of the Moon then causes the IVR to leave the disk, preventing further resonant growth of I; the subsequent system evolution is determined by tidal interaction with the Earth and Sun[5,6,10]. Figure 2 shows I_{max} resulting from a variety of choices of $M_{disk}(0)$ and $t_{spread}(0)$.

Until now, an apparent deficiency of the impact hypothesis has been its inability to account for the inclination of the lunar orbit[23]. Here we identify a resonance that would naturally result as the Moon recoiled from an interior disk; this resonance could, for a range of plausible conditions, yield the requisite lunar inclination. The resulting inclination depends mainly on two parameters: $M_{disk}(0)$ and $t_{spread}(0)$. Simulations of potential Moon-forming impacts by Cameron[9] yield $M_{disk} < 1.5-2\ M_{Moon}$, with somewhat more than half of the mass exterior to a_{Roche}. Forming the Moon at the outer edge of such a disk would leave an inner remnant disk of $0.5-1\ M_{Moon}$. An inner disk whose spreading rate is regulated by its radiative cooling time with a nominal photospheric temperature of 2,000 K will have $t_{spread}(0) < 50(M_{disk}/M_{Moon})$ years. These values coincide well with those needed to yield $I_{max} < 10°$. The inclination of the Moon's orbit may thus represent an important clue to the early state of the post-impact system; we expect that this will motivate further modelling of the physics of an impact-generated protolunar disk. $\qquad\qquad\qquad\qquad\qquad$ M

1. Cameron, A. G. W. & Ward, W. R. The origin of the Moon. *Lunar Sci.* VII, 120–122 (1976).
2. Hartmann, W. K. & Davis, D. R. Satellite-sized planetesimals and lunar origin. *Icarus* 24, 504–515 (1975).
3. Canup, R. M. & Esposito, L. W. Accretion of the Moon from an impact-generated disk. *Icarus* 119, 427–446 (1996).
4. Ida, S., Canup, R. M. & Stewart, G. Formation of the Moon from an impact-generated disk. *Nature* 389, 353–357 (1997).
5. Goldreich, P. History of the lunar orbit. *Rev. Geophys.* 4, 411–439 (1966).
6. Touma, J. & Wisdom, J. Evolution of the Earth-Moon System. *Astron. J.* 108, 1943–1961 (1994).
7. Cameron, A. G. W. & Benz, W. The origin of the Moon and the single impact hypothesis IV. *Icarus* 92, 204–216 (1991).
8. Cameron, A. G. W. The origin of the Moon and the single impact hypothesis V. *Icarus* 126, 126–137 (1997).
9. Cameron, A. G. W. & Canup, R. M. The giant impact occurred during Earth accretion. *Lunar Planet. Sci.* XXIX, 1062–1063 (1998).
10. Touma, J. & Wisdom, J. Resonances in the early evolution of the Earth-Moon system. *Astron. J.* 115, 1653–1663 (1998).
11. Ward, W. R. & Cameron, A. G. W. Disc evolution within the Roche limit. *Lunar Planet. Sci.* IX, 1205–1207 (1978).
12. Kokubo, E., Ida, S. & Makino, J. Evolution of a circumterrestrial disk and formation of a single moon. *Icarus* (submitted).
13. Thompson, C. & Stevenson, D. Gravitational instability in two-phase disks and the origin of the Moon. *Astrophys. J.* 333, 542–481 (1983).
14. Shu, F. in *Planetary Rings* (eds Greenberg, R. & Brahic, A.) 513–561 (Univ. Arizona Press, Tucson, 1984).
15. Elliot, J. L. & Nicholson, P. D. in *Planetary Rings* (eds Greenberg, R. & Brahic, A.) 25–72 (Univ. Arizona Press, Tucson, 1984).
16. Goldreich, P. & Tremaine, S. Disk-satellite interactions. *Astrophys. J.* 241, 425–441 (1980).
17. Borderies, N., Goldreich, P. & Tremaine, S. Excitation of inclinations in ring-satellite systems. *Astrophys. J.* 284, 429–434 (1984).
18. Ward, W. R. & Hahn, J. M. Damping of orbital inclinations by bending waves. *Icarus* 110, 95–108 (1994).
19. Meyer-Vernet, N. & Sicardy, B. On the physics of resonant disk-satellite interaction. *Icarus* 69, 157–175 (1987).
20. Ward, W. R. & Hahn, J. M. The eccentricity of Neptune and the nature of the Kuiper belt. *Science* 280, 2104–2106 (1998).
21. Tremaine, S. Resonant relaxation in protoplanetary disks. *Astron. J.* 116, 2015–2022 (1998).
22. Brouwer, D. & Clemence, G. M. *Methods of Celestial Mechanics* (Academic, New York, 1961).
23. Boss, A. P. & Peale, S. J. in *Origin of the Moon* (eds Hartmann, W. K., Phillips, R. J. & Taylor, G. J. (Lunar and Planetary Institute Press, Houston, 1986).

···

Preparing pure photon number states of the radiation field

B. T. H. Varcoe*, S. Brattke*†, M. Weidinger* & H. Walther*†

* *Max Planck Institute for Quantum Optics, Hans-Kopfermann Strasse 1, D-85748 Garching, Germany*
† *Sektion Physik der Universität München, 85748 Garching, Germany*

···

The quantum mechanical description of a radiation field is based on states that are characterized by the number of photons in a particular mode; the most basic quantum states are those with fixed photon number, usually referred to as number (or Fock) states. Although Fock states of vibrational motion can be observed readily in ion traps[1], number states of the radiation field are very fragile and difficult to produce and maintain. Single photons in multi-mode fields have been generated using the technique of photon pairs[2,3]. But in order to generate these states in a cavity, the mode in question must have minimal losses; moreover, additional sources of photon number fluctuations, such as the thermal field, must be eliminated. Here we observe the build-up of number states in a high-Q cavity, by investigating the interaction dynamics of a probe atom with the field. We employ a dynamical method of number state preparation that involves state reduction of highly excited atoms in a cavity, with a photon lifetime as high as 0.2 seconds. (This set-up is usually known as the one-atom maser or 'micromaser'.) Pure states containing up to two photons are measured unambiguously.

Number states are also generated as trapping states in a micromaser[4]; however, it is not easy to study the purity of the generated states in that case. There are many experiments where single-photon exchange between subsequent atoms has been investigated (see, for example, refs 5 and 6) leading to an entanglement between subsequent atoms and possibly the photons. In those experiments, no state reduction of the photon field in the cavity is performed, and so the field itself is in a more complicated state. During the review process of this Letter, work[7] describing quantum non-demolition measurement of states containing an average of one or zero photons in the mode related to a parity measurement of the photon state was published (see ref. 8 for comparison).

In the micromaser, highly excited atoms (usually called Rydberg atoms) interact with a single mode of a superconducting cavity with a quality factor as high as 3×10^{10}, leading to the above-mentioned photon lifetime. The steady-state field generated in the micromaser has been the subject of many detailed studies, such as the observation of sub-poissonian photon statistics[9]. The dynamics of the atom–field photon exchange has also been investigated in the

collapse and revivals of the Rabi nutation[10], atom interference[11], bistability and quantum jumps of the field[12], atom–field and atom–atom entanglement[13].

The generation of number states in the micromaser has long been anticipated[13,14]. In this connection trapping states were of interest, as, under certain conditions, the 'trapped' steady-state field represents number states. We briefly discuss here the essential features of trapping states of the micromaser field, as our results will also be compared with those expected for the trapping situation.

The interaction of a two-level atom with a single mode of the cavity field is the model system described by the Jaynes–Cummings hamiltonian[15]. In this model, an atom in the presence of a resonant quantum field undergoes Rabi oscillations. Trapping states occur when the atom–field coupling, Ω, and the interaction time, t_{int}, are chosen such that in a cavity field with n photons each atom undergoes an integer number, k, of Rabi cycles. This is summarized by the condition:

$$\Omega\, t_{int} \sqrt{n+1} = k\pi \qquad (1)$$

Rubidium oven

Stark shifting plates

Auxiliary detector

Reference laser

Velocity selecting ultraviolet laser

Piezos for fine adjustment of the niobium resonator

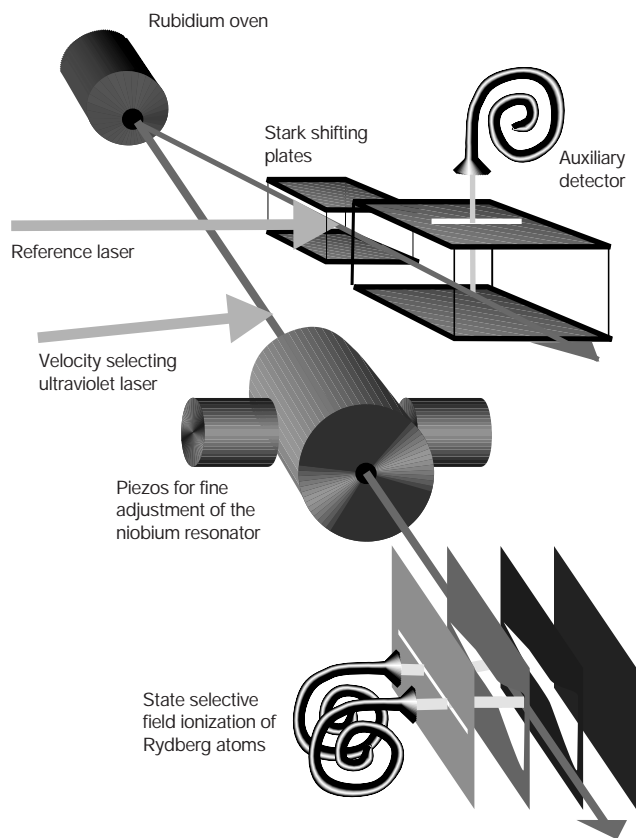State selective field ionization of Rydberg atoms

Figure 1 The experimental set-up. A frequency-doubled dye laser ($\lambda = 297$ nm) was used to excite rubidium ^{85}Rb atoms to the Rydberg $63P_{3/2}$ state from the $5S_{1/2}$ ($F = 3$) ground state. The maser cavity is tuned to the $63P_{3/2}$–$61D_{5/2}$ (21.456 GHz) transition and tuning of the cavity is performed with two piezo translators. Velocity selection is provided by angling the excitation laser towards the main atomic beam at 11° to the normal. The dye laser was locked to a reference beam, using an external computer control, to the $5S_{1/2}$–$63P_{3/2}$ transition of the reference atomic beam excited under normal incidence. In order to obtain controlled continuous tuning of the laser frequency, and hence the atomic velocity, a Stark field was applied to the reference beam. This Stark field was produced by means of a high-quality programmable power supply. The cavity is cooled below 300 mK by the cryostat, corresponding to a maximum thermal photon number of 0.033. For interaction times below 40 µs the excitation spectra of $63P_{1/2}$ and $63P_{3/2}$ levels overlap, leading to excitation of $63P_{1/2}$ atoms which do not interact in the cavity field; however, they are counted in the detectors leading to a perturbation of the counting statistics. The Rydberg atoms are detected by field ionization in two detectors set at different voltages so that the upper and lower states, $63P_{3/2}$ and $61D_{5/2}$, can be counted separately.

When this condition is satisfied, the photon number is left unchanged following the interaction of an atom with the field and the photon number is therefore trapped[16]. It has been demonstrated[4] that trapping states up to $n = 5$ are present. In the trapping states, whenever a photon is lost from the field due to dissipation, the next excited-state atom entering the cavity will emit a photon with a high probability and restore the photon number.

Here we report on an alternative method of generating number states. This method has the advantage that the generated states can be analysed in an unambiguous way afterwards. In the usual operation of the micromaser, atoms in the upper state of the maser transition are injected into the cavity. In the absence of dissipation, atoms detected in the lower state must have emitted a single photon into the cavity field. The interaction of an atom with a field that is initially in the vacuum state $|0\rangle$, or more generally in a state $|n\rangle$, changes the field state to a superposition of the states $|n\rangle$ and $|n + 1\rangle$. By measuring an atom in the ground state, the superposition is reduced to the state $|n + 1\rangle$. Therefore the determination of the state of all outgoing atoms reduces the state of the cavity field to a pure number state[17]. Without state reduction a mixture of the $|n\rangle$ and $|n + 1\rangle$ states would persist in the cavity. The presence of dissipation complicates the discussion and as a result a fixed number state is not precisely reached (see the data analysis below).

In the presence of a cavity photon number, $|n\rangle$, the relative populations of the excited and ground states of an atom will oscillate at a frequency $\Omega\sqrt{n+1}$. Experimentally the atomic inversion, given by $I = P_g - P_e$, is measured. Here P_g and P_e are the probability of finding a ground-state or excited-state atom, respectively. If the
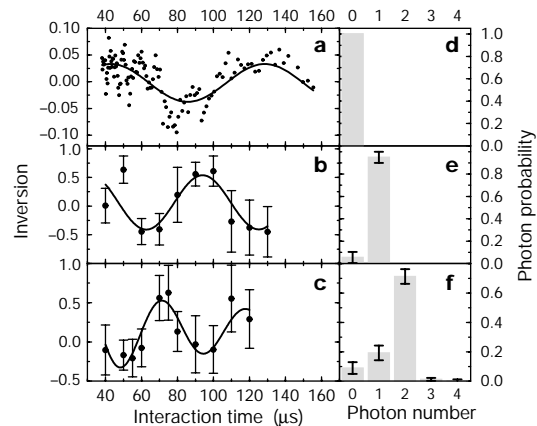

Figure 2 Three Rabi oscillations. **a**, **b** and **c** represent the number states $n= 0$, 1 and 2, respectively. The plots in **d**, **e** and **f** display the coefficients P_n. The photon distribution P_n was calculated for each Rabi cycle by fitting equation (2) to each plot for the set of photon numbers $n = 0$ to $n = 3$. The relative phase of the Rabi frequency was fixed because all the atoms enter in the excited state of the maser transition. In each fit the highest probability was obtained for the target number state. Unlike the $n = 1$ and $n = 2$ Rabi cycles, the $n = 0$ oscillation in **a** was obtained in the steady-state operation of the micromaser in a very low-flux regime. The fit to this curve was performed for Rabi cycles from $n = 0$ to $n = 2$. The low visibility of this curve was due to the low flux (<1 Hz) which was required to reduce the steady-state operation of the micromaser to below-threshold behaviour; hence, detector dark counts become comparable to the real count rates and therefore contribute to a large background. To improve the measurements for photon number of $n = 3$ and higher, the range of interaction times would have to be extended beyond 120 µs, but this is not possible with the current apparatus. During the Rabi cycle the cavity photon number changes periodically. At each maximum there is one photon more than at the minimum. The Rabi oscillation thus allows a non-destructive and repeated measurement of the photon number to be performed. See refs 7 and 8 for comparison. In connection with the discussion of trapping states, it is interesting to note that minima in the number-state Rabi oscillations correspond precisely to the trapping-states conditions of the steady-state field[4]. Therefore the large possible storage times of single photons would permit investigation of the transition from a pulsed to a steady-state experiment.

field is not in a number state the inversion is given by:

$$I(t_{int}) = -C \bigwedge_n P_n \cos(2 \cdot \sqrt{n+1} t_{int}) \qquad (2)$$

Here P_n is the probability of finding n photons in the mode and t_{int} is the interaction time of the atoms with the cavity field. Rabi cycling of a probe atom can therefore be used as an unambiguous test of the photon distribution in the cavity by analysing the dynamics using equation (2). The factor C considers the reduction of the signal amplitude as a result of dark counts.

The experimental apparatus of the micromaser used for the present experiment is presented in Fig. 1. The present set-up has been described in detail[4,12]. The natural velocity distribution of the atomic beam allowed the interaction time of the atoms with the cavity to be tuned from 40 μs to 160 μs. There was an uncertainty in the interaction time of at most 3%. The cavity used for the measurement described here had a Q factor of 3.4×10^9, corresponding to a photon lifetime of 25 ms. A higher Q value would have increased the measuring time as discussed below.

In contrast to previous experiments with the micromaser, pulsed excitation of the atoms is used so that the number of atoms passing through the cavity can be predetermined. The probability of detecting an atom in either the excited or ground state is about 40% with a 3–5% miscount rate. Owing to the finite lifetime of the atoms, additional atoms are lost through spontaneous emission in the flight between the cavity and the detectors[4]. To create and detect an n-photon number state in the cavity, $N = n + 1$ atoms are required. That is n atoms to create the number state and the final atom as a probe of the state. However, owing to the non-perfect detector efficiency and atomic decay there are missed counts. By using a laser pulse of short duration the number of excited-state atoms entering the cavity per pulse is low. Hence we know that when N atoms per pulse were detected the probability of having $N + 1$ atoms per pulse was negligibly small. This was achieved by modifying the ultraviolet excitation pulse such that the mean number of atoms per pulse was between 0.2 and 0.8. With 40% detector efficiency and the assumption that the probability of missing a count is statistically independent, there is a probability of about 1% of the state preparation being incorrect because an atom escapes detection[18]. As the flux of atoms was variable, the pulse duration was also variable; a maximum sampling time of 3 ms for the $n = 1$ data and 5 ms for the $n = 2$ data was imposed to limit the time delay between the pump and probe atoms. In fact, in most cases the time delay was comparable to the excitation pulse duration. For the

measurement of an n-photon number state, the detection of the probe atom is triggered by the detection of n ground-state atoms within the length of the laser pulse. If too few or too many atoms (upper- or lower-state) are detected within the laser pulse duration, the measurement is rejected.

To ensure that the cavity is in the vacuum state at the start of a measurement, there is a delay of 1.5 cavity decay times between the laser pulses. Hence we compromised with a Q value lower than ultimately possible in our set-up, because a higher Q would lead to an increase of the data collection time. Even with the reduced cavity lifetime of 25 ms and large delay times between the laser pulses, a cyclically steady-state maser field can build up in the cavity. The time delay between pulses was selected as a compromise between limiting the growth of the maser field and the length of the data collection time.

Figure 2a–c displays three Rabi cycles obtained by measuring the inversion of a probe atom that followed the detection of $n = 0$, 1 or 2 ground-state atoms respectively. Figure 2d–f displays normalized values of the coefficients P_n obtained from these curve fits. The strongest indication that the data in Fig. 2a–c represent three number states is provided in Fig. 3, where the frequency of single sine wave curve fit is plotted for each graph alongside the theoretical variation of the Rabi frequency as a function of the photon number. There is a small dependence of the coupling constant on atom–field detuning and our day-to-day repeatability of the detuning is limited to a few kilohertz. The photon probabilities in Fig. 2d–f therefore use the frequency plotted in Fig. 3 as a reference frequency to calculate the frequencies for other possible number-state components. A similar method[19], using the interaction between the atoms and field, was used to analyse a coherent microwave field injected into a cavity.

The simulations, which are described later, demonstrate that we produced number states with a purity of 99% for the $n = 1$ state and 95% for the $n = 2$ state. The fact that we do not measure pure number states is caused by dissipation in the time interval between production and analysis of the cavity field.

Because of the long waiting times for three atom events, the $n = 2$ Rabi data were more difficult to collect than the other two measurements. The data collection time became substantially longer as the interaction time was increased and background effects have a higher impact on the data. The fit to the $n = 2$ data includes an exponentially decreasing weight, so that measurements obtained for longer interaction times have less significance than those at short times.
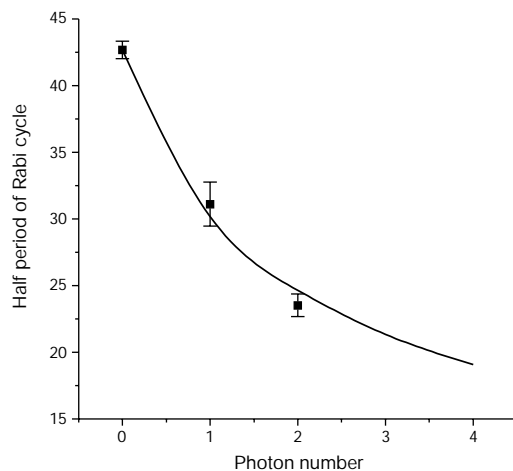

Figure 3 Dependence of the Rabi frequency on the photon number. A single sine fit to each of the three curves in Fig. 2a–c is plotted versus the theoretical variation of frequency as a function of photon number. The theoretical plot was calculated for the coupling constant of 36.8 krad s^{-1}, which was the best fit to the data.
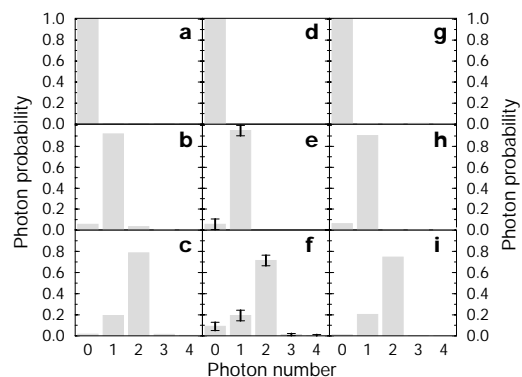

Figure 4 Theoretical and experimental results on the purity of number states. **a–c**, A theoretical simulation of the current experiment; **d–f**, the current experimental results; **g–i**, a theoretical model that extends the current experiment to the steady state at the positions of the trapping states. The agreement between the two theoretical results and the experimental result is remarkable, indicating that dissipation is the most likely loss mechanism. Without dissipation (that is, in the moment of generation) the purity of the states is 99% for $n = 1$ and 95% for $n = 2$.

The limited resolution of the $n = 1$ and $n = 2$ Rabi oscillations is a result of the cumulative effect of velocity and detuning fluctuations, a 3–5% miscount rate in the state-selective detectors and detector dark counts. The presence of number states, however, can be determined independently of the resolution because the only important factor is the accumulated Rabi phase of the probe atom as it passes through the cavity. The data for the $n = 1$ and $n = 2$ Rabi oscillations were evaluated considering possible disturbances by trapping states.

We now calculate the dissipation of the field before detection in order to determine the influence of dissipation. For these simulations we make two idealizing assumptions: thermal photons are only taken into account for the long-term build-up of the cyclically steady state, and gaussian averaging over velocity spread of atoms is considered to be about 3%. Considered in the calculations are the exponential decays for the cavity field during the pulse when either one photon (for $n = 1$) or two photons were deposited one by one (for $n = 2$) changing the photon number distribution. The simulations also average over the poissonian arrival times of the atoms. The details of this calculation will be discussed elsewhere (B. T. H. V. et al., manuscript in preparation). The results of these calculations are compared to the experimental results in Fig. 4a–f.

As dissipation is the dominant loss mechanism, it is interesting to compare the purity of the number states generated by the current method with that expected for trapping states (Fig. 4g–i). The agreement of the purity of the number states is very good. The trapping-state photon distribution is generated in the steady state, which means that whenever the loss of a photon occurs the next incoming atom will restore the old field with a high probability. The non-zero amplitudes of the states $|0\rangle$ in Fig. 4h and $|1\rangle$ in Fig. 4i are due to dissipative losses before restoration of a lost photon, which is not replaced immediately but after a time interval dependent on the atom flux. The atom rate used in these calculations was 25 atoms per cavity decay time, or an average delay of 1 ms. This can be compared to the delay between the preparation and probe atoms in the present experiment. In the steady-state simulation loss due to cavity decay determines the purity of the number state; in the limit of zero loss the state measurement is perfect. We conclude that dissipative loss due to cavity decay in the delay to a probe atom largely determines the measured deviation from a pure number state. The thermal field also influences the photon distribution. The nature of the selection process in the current experiment means that we can reduce the influence of the thermal field by only performing measurements of the field state after a trigger of n ground state atoms. Hence, the state of the field is well known. The steady-state simulation was therefore performed for a temperature of 100 mK, which makes the influence of the thermal field in the steady-state correspondingly low.

The fact that number states can be readily created presents many opportunities. For example, in connection with the investigation of quantum information, the decoherence of 'Schrödinger cat' states can be largely attributed to dissipation. The very low influence of dissipation in this experiment provides an excellent environment for investigating decoherence and non-local quantum phenomena such as entanglement of atoms. ▪

1. Leibfried, D. et al. Experimental determination of the motional quantum state of a trapped atom. Phys. Rev. Lett. 77, 4281–4285 (1996).
2. Hong, C. K. & Mandel, L. Experimental realization of a localized one photon state. Phys. Rev. Lett. 56, 58–60 (1986).
3. Fearn, H. & Loudon, R. Theory of two-photon interference. J. Opt. Soc. Am. B 6, 917–927 (1989).
4. Weidinger, M., Varcoe, B. T. H., Heerlein, R. & Walther, H. Trapping states in the micromaser. Phys. Rev. Lett. 82, 3795–3798 (1999).
5. Maître, X. et al. Quantum memory with a single photon in a cavity. Phys. Rev. Lett. 79, 769–772 (1997).
6. Englert, B. et al. Entangled atoms in micromaser physics. Fortschr. Phys. 46, 897–926 (1998).
7. Nogues, G. et al. Seeing a single photon without destroying it. Nature 400, 239–242 (1999).
8. Englert, B.-G., Sterpi, N. & Walther, H. Parity States in the one-atom maser. Opt. Commun. 100, 526–535 (1993).
9. Rempe, G. & Walther, H. Sub-poissonian atomic statistics in a micromaser. Phys. Rev. A 42, 1650–1655 (1990).
10. Rempe, G., Walther, H. & Klein, N. Observation of quantum collapse and revival in the one-atom maser. Phys. Rev. A 58, 353–356 (1987).
11. Raithel, G., Benson, O. & Walther, H. Atomic interferometry with the micromaser. Phys. Rev. Lett. 75, 3446–3449 (1995).
12. Benson, O., Raithel, G. & Walther, H. Quantum jumps of the micromaser field - dynamic behavior close to phase transition points. Phys. Rev. Lett. 72, 3506–3509 (1994).
13. Filipowicz, P., Javanainen, J. & Meystre, P. Theory of a microscopic maser. J. Opt. Soc. B 34, 3077–3087 (1986).
14. Cummings, F. W. & Rajagopal, A. K. Production of number states of the electromagnetic field. Phys. Rev. A 39 3414–3416 (1989).
15. Jaynes, E. T. & Cummings, F. W. Quantum and semiclassical radiation theories. Proc. IEEE 51, 89–109 (1963).
16. Meystre, P., Rempe, G. & Walther, H. Very-low temperature behavior of a micromaser. Opt. Lett. 13, 1078–1080 (1988).
17. Krause, J., Scully, M. O. & Walther, H. State reduction and $|n\rangle$-state preparation of a high-Q micromaser. Phys. Rev. A 36, 4547–4550 (1987).
18. Wehner, E., Seno, R., Sterpi, N., Englert, B.-G. & Walther, H. Atom pairs in the micromaser. Opt. Commun. 110, 655–669 (1994).
19. Brune, M. et al. Quantum Rabi oscillation: A direct test of field quantisation in a cavity. Phys. Rev. Lett. 76, 1800–1803 (1996).

Imaging the effects of individual zinc impurity atoms on superconductivity in $Bi_2Sr_2CaCu_2O_{8+\delta}$

S. H. Pan*†, E. W. Hudson*, K. M. Lang*, H. Eisaki‡§, S. Uchida‡ & J. C. Davis*

* Department of Physics, University of California, Berkeley, California 94720, USA
‡ Department of Superconductivity, University of Tokyo, Tokyo 113-8656, Japan
§ Department of Applied Physics, Stanford University, Stanford, California 94305, USA

Although the crystal structures of the copper oxide high-temperature superconductors are complex and diverse, they all contain some crystal planes consisting of only copper and oxygen atoms in a square lattice: superconductivity is believed to originate from strongly interacting electrons in these CuO_2 planes. Substituting a single impurity atom for a copper atom strongly perturbs the surrounding electronic environment and can therefore be used to probe high-temperature superconductivity at the atomic scale. This has provided the motivation for several experimental[1–8] and theoretical studies[9–20]. Scanning tunnelling microscopy (STM) is an ideal technique for the study of such effects at the atomic scale, as it has been used very successfully to probe individual impurity atoms in several other systems[21–25]. Here we use STM to investigate the effects of individual zinc impurity atoms in the high-temperature superconductor $Bi_2Sr_2CaCu_2O_{8+\delta}$. We find intense quasiparticle scattering resonances[26] at the Zn sites, coincident with strong suppression of superconductivity within ~15 Å of the scattering sites. Imaging of the spatial dependence of the quasiparticle density of states in the vicinity of the impurity atoms reveals the long-sought four-fold symmetric quasiparticle 'cloud' aligned with the nodes of the d-wave superconducting gap which is believed to characterize superconductivity in these materials.

† Present address: Department of Physics, Boston University, Boston, Massachusetts 02215, USA.